Infrared nanoscopy down to liquid helium temperatures

Denny Lang, Jonathan Döring, Tobias Nörenberg, Ádám Butykai, István Kézsmárki, Harald Schneider, Stephan Winnerl, Manfred Helm, Susanne C. Kehr, Lukas M. Eng

Angaben zur Veröffentlichung / Publication details:

Lang, Denny, Jonathan Döring, Tobias Nörenberg, Ádám Butykai, István Kézsmárki, Harald Schneider, Stephan Winnerl, Manfred Helm, Susanne C. Kehr, and Lukas M. Eng. 2018. "Infrared nanoscopy down to liquid helium temperatures." *Review of Scientific Instruments* 89 (3): 033702. https://doi.org/10.1063/1.5016281.

Infrared nanoscopy down to liquid helium temperatures

Denny Lang,[1,2,a)] Jonathan Döring,[2,b)] Tobias Nörenberg,[2] Ádám Butykai,[3] István Kézsmárki,[3,4] Harald Schneider,[1] Stephan Winnerl,[1] Manfred Helm,[1,2,5] Susanne C. Kehr,[2] and Lukas M. Eng[2,5]

[1]*Helmholtz-Zentrum Dresden-Rossendorf, Institute of Ion Beam Physics and Materials Research, 01328 Dresden, Germany*
[2]*Institute of Applied Physics, Technische Universität Dresden, 01062 Dresden, Germany*
[3]*Department of Physics, Budapest University of Technology and Economics and MTA-BME Lendület Magneto-Optical Spectroscopy Research Group, 1111 Budapest, Hungary*
[4]*Experimental Physics V, Center for Electronic Correlations and Magnetism, Institute of Physics, University of Augsburg, 86135 Augsburg, Germany*
[5]*cfaed—Center for Advancing Electronics Dresden, Technische Universität Dresden, 01062 Dresden, Germany*

(Received 17 November 2017; accepted 11 February 2018; published online 1 March 2018)

We introduce a scattering-type scanning near-field infrared microscope (s-SNIM) for the local scale near-field sample analysis and spectroscopy from room temperature down to liquid helium (LHe) temperature. The extension of s-SNIM down to $T = 5$ K is in particular crucial for low-temperature phase transitions, e.g., for the examination of superconductors, as well as low energy excitations. The low temperature (LT) s-SNIM performance is tested with CO_2-IR excitation at $T = 7$ K using a bare Au reference and a structured Si/SiO_2-sample. Furthermore, we quantify the impact of local laser heating under the s-SNIM tip apex by monitoring the light-induced ferroelectric-to-paraelectric phase transition of the skyrmion-hosting multiferroic material GaV_4S_8 at $T_c = 42$ K. We apply LT s-SNIM to study the spectral response of GaV_4S_8 and its lateral domain structure in the ferroelectric phase by the mid-IR to THz free-electron laser-light source FELBE at the Helmholtz-Zentrum Dresden-Rossendorf, Germany. Notably, our s-SNIM is based on a non-contact atomic force microscope (AFM) and thus can be complemented *in situ* by various other AFM techniques, such as topography profiling, piezo-response force microscopy (PFM), and/or Kelvin-probe force microscopy (KPFM). The combination of these methods supports the comprehensive study of the mutual interplay in the topographic, electronic, and optical properties of surfaces from room temperature down to 5 K. *Published by AIP Publishing.*
https://doi.org/10.1063/1.5016281

I. INTRODUCTION

In the last decade, scattering-type scanning near-field infrared optical microscopy (s-SNIM) has developed into a powerful and widespread method for the nanoscale imaging and spectroscopic analysis at infrared (IR) and terahertz (THz) wavelengths.[1–5] Providing resolution ways beyond the classical diffraction limit,[6] s-SNIM has valuably contributed to the fields of 2D materials (e.g., graphene[7–9] and MoS_2[10]), to the research of metamaterials and superlenses,[11–13] and to the investigation of semiconductor and organic nanostructures,[2,14] just to mention a few examples. Nevertheless, a lot of prominent effects in solid-state physics such as superconductivity,[15,16] phase transitions in multiferroic materials,[17,18] or the confinement in low-dimensional quantum structures[19] need to be explored at low temperatures (LT). Combining LT with the huge potential of IR and THz nanoscopy thus promises great advances in understanding and probing fundamental excitations, such as phonons, magnons, and polaritons, in these exotic material classes. The goal of this work is to advertise such a promising combination that involves the "FELBE" tunable free-electron laser (FEL) at the Helmholtz-Zentrum Dresden-Rossendorf, Germany, as a high repetition rate, narrow-band light source tunable from 5 to 250 μm wavelength.

To the best of our knowledge, the first work on LT s-SNIM was reported by Moldovan-Doyen *et al.*[20] and used the s-SNIM to collect (rather than excite) mid-IR to THz photons with sub-diffraction resolution at $T = 100$ K, exploring the light emission of an (active) quantum cascade laser element that was coupled to a photonic crystal. Moreover, Yang *et al.*[21] demonstrated LT s-SNIM at $T = 200$ K on non-conducting domains in V_2O_3 single crystals that nucleate around topographic defects. Furthermore, a recent publication by McLeod *et al.*[18] impressively showed the detailed mapping of the V_2O_3 insulator-to-metal transition at $T > 160$ K.

Closely related to s-SNIM, scanning tunneling microscopy (STM) combined with laser illumination at cryogenic temperatures has been developed even earlier. Wu *et al.* reported in 2006 on a home-built STM operating at 9.5 K for the investigation of light-induced electron tunneling of single molecules.[22] Moreover, tip-enhanced Raman spectroscopy studies based on STM at cryogenic temperatures have been demonstrated by Jiang *et al.*[23] and Zhang *et al.*[24] Latest developments

a)Electronic mail: d.lang@hzdr.de
b)J. Döring contributed equally to this work.

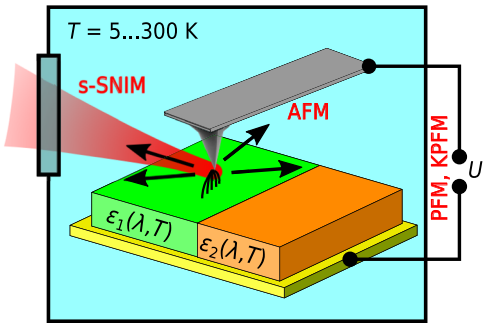

FIG. 1. Sketch of the LT s-SNIM: IR/THz radiation is focused onto the tip-sample junction inside the liquid helium (LHe) cryostat. Elastically backscattered radiation from the tip-sample system is measured and the near-field contributions extracted, which contain the local information of the sample permittivity " as a function of temperature T and wavelength . Both the sample and tip are electrically contacted in order to enable complementary AFM-techniques such as PFM or KPFM.

combine cryogenic STM with strong fs-laser pulses for the tracking of intrinsic tunneling dynamics on the molecular length scale.[25,26]

Our work here demonstrates LT s-SNIM (Fig. 1) operation down to 5 K, while exploring different samples including Au, structured Si-SiO_2, and multiferroic GaV_4S_8 with both the CO_2 laser and the FEL.[3] The overall LT s-SNIM functionality at various temperatures is illustrated by inspecting a topographically planar Au surface as well as a structured Si/SiO_2-sample. We study the multiferroic material GaV_4S_8[27–30] in order to quantify the local impact of IR radiation by the tip-sample confinement. Moreover the local spectral response as well as the lateral distribution of structural domains below 42 K is studied on the same GaV_4S_8 sample by means of *in situ* LT s-SNIM, PFM, and KPFM.[17,30,31]

II. SETUP

A. s-SNIM

In s-SNIM, infrared radiation is scattered by the AFM tip that oscillates a few nm above the sample surface. Due to the tip-sample interaction in the optical near field, the radiation scattered to the far field contains information on the local refractive index tensor of the sample.[6,32]

Our LT s-SNIM is based on a custom-made LT AFM system (by *Attocube Systems AG*) using a *Janis Research Company* liquid helium (LHe) bath cryostat. For s-SNIM measurements, the AFM is operated in tapping-mode,[33] with the cantilever being mechanically excited at its resonance frequency f_0 of about 170 kHz with a typical oscillation amplitude of 50 nm. The actual cantilever motion is detected with a fiber-based homodyne interferometer at λ = 1310 nm. We use standard non-contact AFM cantilevers (*PPP-NCLPt* from *NANOSENSORS*) for all measurements. AFM tips possess a 25 nm PtIr5 coating that enables spectrally flat optical excitation over the whole wavelength range from 5 to 250 μm.[34] Equally, such tips show an excellent thermal and electrical conductivity, e.g., to allow for specific complementary AFM-mode operation such as PFM or KPFM at one and the same sample position.

PFM makes use of the converse piezoelectric effect and thus is able to probe different components of the local piezoelectric tensor of the material under inspection.[31,35,36] Applying a 1–10 kHz AC voltage with a typical amplitude of 1–10 V between the tip and sample in contact-mode of the AFM leads to local distortions and sample oscillations that are sensed by the AFM probe and demodulated via a lock-in amplifier. The lock-in amplifier measures both amplitude A_{PFM} and phase $_{PFM}$ with respect to the excitation. Note that due to the interferometric cantilever detection, only out-of-plane components of the piezoelectric tensor can be addressed in our LT setup.

KPFM, on the other hand, operates in non-contact mode and allows us to locally quantify and compensate any electrostatic potential offset between the tip and sample surface.[37,38] KPFM hence not only minimizes cross talk of electrostatic forces and topography or s-SNIM signals but also equally allows for probing the local work function[39] or sample surface photo-voltage[40] of the sample system simultaneously to s-SNIM investigations. For KPFM, we typically apply a 1 V AC-bias at 4 kHz to the tip on top of the fundamental oscillation amplitude of the cantilever.

B. LT s-SNIM optical setup

The optical setup of our s-SNIM is sketched in Fig. 2(a). As shown, either a narrow-band table-top CO_2 laser or the FEL at Helmholtz-Zentrum Dresden-Rossendorf are used as IR excitations. The FEL wavelength is tunable over a broad range from 5 μm to 250 μm (2000 cm ^{1} to 40 cm ^{1}, 60 THz to 1.2 THz, or 248 meV to 5 meV) and provides a 1-25 ps pulse train at a repetition rate of 13 MHz. The typical spectral width is about 1% of the actual wavelength, which allows for s-SNIM imaging with narrow-band excitation. The tunability of the continuous wave (cw) CO_2 laser is limited to various sharp lines between 9.6 μm and 11.4 μm.

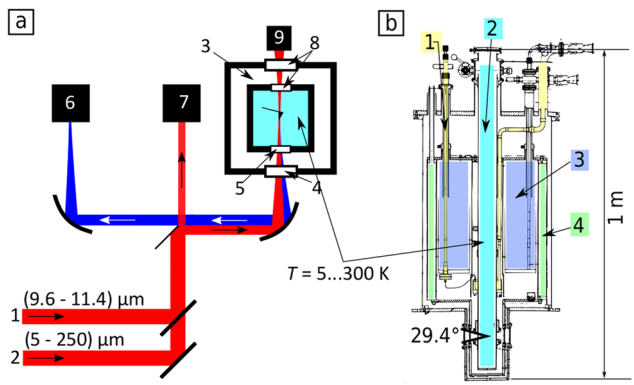

FIG. 2. (a) Scheme of the optical setup, combined with the LT s-SNIM: the tunable infrared laser source [CO_2 laser (1) or FEL (2)] is focused on the tip-sample system in the cryostat (3) through an outer window [(4); KRS5, quartz, or ZnSe] and an inner diamond window (5). The backscattered radiation is again focused on and detected by a infrared/THz detector [(6); MCT, Ge:Ga detector, or hot-electron bolometer]. The laser power is recorded simultaneously by a powermeter (7). The quartz windows (8) enable optical access for alignment and positioning by a camera (9). (b) Cryostat with a heat-exchange system (1), sample tube (2) filled with He exchange gas at 100 mbar containing the AFM (not shown here), and LHe (3) and LN_2 (4) Dewar vessels.

After passing a geometric beam-splitter (BS), half of the incident radiation is directed to a power meter to monitor the stability of the incident beam. The power at the position of the LT s-SNIM probe, calculated from the measured power by subtracting the reflection losses at the cryostat windows, is typically in the order of 10–50 mW. The other part of the beam is focused onto the tip apex using a 3^{00} Au-coated parabolic mirror sitting outside of the cryostat, with a resulting numerical aperture of about 0.2 and a focus diameter of about 100 μm at the s-SNIM probe for $\lambda = 10$ μm. Both the incident and the backscattered radiation pass through two cryostat windows: an outer window made of KRS-5, ZnSe, or quartz for different wavelength regimes, respectively, and an inner diamond window. This results in a total attenuation of about 50% for every direction. For all measurements presented here, the radiation is polarized parallel to the incident plane (p-pol) of the tip-sample system, which results in the strongest near-field response.[6] Nevertheless, it is possible to rotate the polarization by 90 resulting in perpendicular (s-pol) polarization with respect to the incident plane.

Note that in order to avoid strong spectral variations of the laser power at the position of the tip, except for the cryostat windows we exclusively use non-dispersive optics such as reflection optics for focusing and change of polarization. Moreover, the complete setup may be purged by dry nitrogen to reduce absorption by ambient air.

The backscattered radiation, that carries the information about the refractive index of the sample on the local scale, is collected by the same parabolic mirror and, after passing through the BS, is focused onto the detector. Depending on the wavelength, we use either a photoconductive mercury cadmium telluride (MCT) detector (4 μm $< \lambda <$ 26 μm), a LHe-cooled gallium doped germanium (Ge:Ga) photoconductive detector (24 μm $< \lambda <$ 50 μm), or a LHe-cooled indium anitmonide (InSb) hot-electron bolometer (50 μm $< \lambda <$ 250 μm). The detector output is demodulated at the n-th harmonic of the cantilever resonance frequency using a lock-in amplifier. The resulting signals are further referred to as NF_n . This technique effectively suppresses far-field components in the detected signal.[6,41,42]

C. Cryostat

The bath cryostat [see Fig. 2(b)] consists of two Dewar vessels for liquid nitrogen and liquid helium allowing for LT measurements down to $T = 5$ K. The inner tank connects to the sample tube via a heat exchanger, where the liquid helium cools the outer wall of the sample tube. The sample tube hosts the AFM and is filled with He gas at a pressure of about 100 mbar in order to facilitate heat transfer between the sample and the wall.

Two thermosensors combined with heating elements are located directly below the sample holder as well as on the wall of the sample tube at the height of the tip. Whenever the temperature at both thermosensors is equal, the system is in a thermal equilibrium, which is the starting point for all LT s-SNIM investigations. The temperature measured at the sample holder is hereafter labeled as T_s, whereas the actual temperature on the sample beneath the tip can differ due to local laser heating as discussed later. The temperature T_s is controlled by the flow of liquid gas and a temperature controller connected to both heating elements.

The optical access to the cryostat is provided in two separate paths: the near-field s-SNIM path (excitation and detection) is coupled in via the parabolic mirror and is focused onto the AFM tip as described above, while the monitoring and adjustment path hosts an optical camera mounted at the rear exit of the cryostat (see Fig. 2).

III. RESULTS

A. LT s-SNIM performance

We verify the near-field performance of our LT s-SNIM system by probing a structured Si/SiO_2-sample (for details see the Appendix) at a nominal temperature of $T_s = 7$ K using the CO_2 laser at a wavelength of $\lambda = 9.7$ μm (see Fig. 3). Note that this sample system has been chosen deliberately to reveal a s-SNIM contrast that is temperature independent and thus can be compared with room temperature results.[43]

A topography scan of this sample is depicted in Fig. 3(a) with a zoomed-in sector (white rectangle) shown in Fig. 3(c). The higher, bright areas represent SiO_2 whereas the lower, dark areas correspond to Si. The scanned section contains stripes and rectangles of different sizes. Note that the smallest of them are even on the magnitude of the probe's apex diameter of about 50 nm. We obtain a RMS-roughness of 0.5 nm on SiO_2, which proves the excellent AFM stability at low temperatures. The corresponding, simultaneously recorded near-field signal [Fig. 3(b) with zoom Fig. 3(d)] reveals an inverted optical

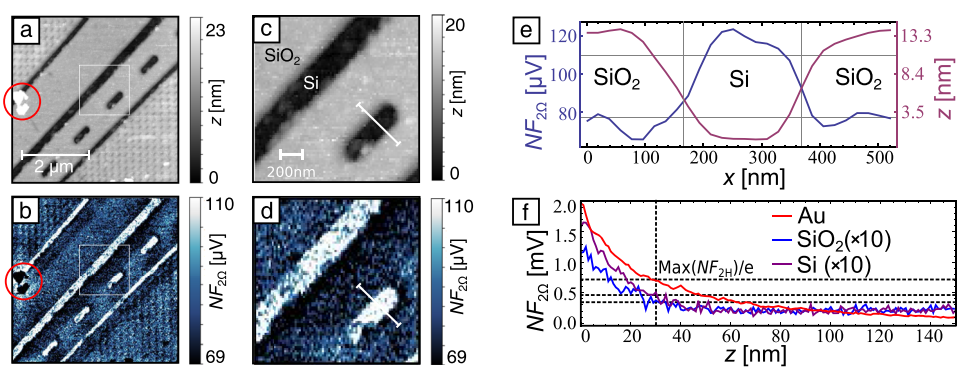

FIG. 3. Topography (a) and near-field (b) scans at $T_s = 7$ K of structured Si-SiO_2 with associated zoom areas (c) and (d). The corresponding profiles (e) demonstrate a spatial LT s-SNIM resolution better than 100 nm. The measured retract curves (f) of Au (reference), Si, and SiO_2 confirm the near-field characteristics[6] of the measurements with a non-linear decay of NF_2 within about 30 nm at Max.

contrast with respect to the topography: Here the SiO_2 areas appear darker than the Si areas. This can be explained by the values of the wavelength-dependent permittivities of both materials taking $\varepsilon_{Si} = 11.8 + 3 \quad 10^{-4}i$[44] and $\varepsilon_{SiO_2} = 6.4 + 7.9i$[45] for $\lambda = 9.7$ μm resulting in higher and lower s-SNIM signals, respectively.[6] The signal-to-noise ratio of NF_2 for SiO_2 is approximately 9 and even the smallest structures are clearly visible (top-left and bottom-right areas). Residual particles on the scan, that can neither be assigned to SiO_2 nor to Si, appear dark in the near-field image [see red circle in Figs. 3(a) and 3(b)]. This indicates that they are most likely highly insulating and being nonresonant with respect to the excitation wavelength.

A more detailed view is presented in the cross section profile in Fig. 3(e). The Si-SiO_2 edge in the topography shows a width of less than 100 nm in the AFM. Notably, the spatial resolution of NF_2 is similar. To verify the near-field character of NF_2 , we compare its dependence on the tip-sample distance by retract curves on Si, SiO_2, and Au, respectively, as depicted in Fig. 3(f). Both for Si and SiO_2, NF_2 is more than 10 times smaller than for the plane Au reference sample since Au, as a metal, is highly reflective ($\varepsilon_{Au} = -4330 + 757i$[46]), which results in a huge near-field signal. On all three materials, a non-linear decay of NF_2 , typical for the near field, is observed within 30 nm at Max $(NF_{2H})/e$. This decay is known to scale with the tip diameter[6] and therefore is in good agreement with the observed spatial resolution better than 100 nm.

B. Temperature calibration

The sample temperature T_s of our LT s-SNIM system is measured below the sample holder and is thus accurate for samples with excellent thermal conductivity like metals. However, the temperature of the sample at the local position of the tip may be higher due to local heating by the focused infrared laser and additionally due to the field enhancement at the tip apex of the metallic probe. This heating effect is expectedly influenced by sample parameters such as thermal conductivity and wavelength-dependent infrared absorption. Especially the latter will play an important role for the s-SNIM investigation of materials close to absorption resonances, for instance, within the reststrahlen band. Measurements in this regime are of particular interest for s-SNIM since the near-field enhancement conditions result in an enhanced sample sensitivity.[1,47]

In order to determine experimentally the local sample heating at the tip induced by the infrared laser, the Jahn-Teller transition in multiferroic GaV_4S_8 is used.[28,30] This material becomes ferroelectric below a critical temperature $T_c = 42$ K,[30] which induces a clear contrast in the PFM-signal [see Fig. 4(d)] due to ferroelectric domains with polarizations pointing along any of the four ħ111i-type axes. Figures 4(a)–4(c) show topography and PFM images of the (111) surface of a GaV_4S_8 single crystal at $T_s = 20$ K, which clearly display the lamellar ferroelectric domain pattern. We measure the out-of-plane piezoelectric tensor components discussed in detail by Butykai *et al.*[30]

We study the effect of local heating with a CO_2 laser at 10.6 μm. Starting with various temperatures $T_s < T_c$, the sample is locally heated by the CO_2 laser. We monitor the temperature T_s by the two thermosensors of the cryostat starting in thermal equilibrium. Here, a 2D image of PFM amplitude (A_{PFM}) and PFM phase ($_{PFM}$) of the GaV_4S_8 sample is recorded to obtain the domain pattern and to chose a suitable line with clear domain contrast [Fig. 4(d)]. During calibration, this line is scanned repeatedly while the laser power P_t is increased gradually until the domains disappear in the PFM-signals at a critical laser power P_c. For $P_t > P_c$, the sample is locally heated up to the paraelectric phase; hence, the domains vanish leading to zero A_{PFM} and random $_{PFM}$ signals. At the transition point, the local temperature due to laser heating reaches T_c. Consequently, the difference $T = T_c - T_s$ is the

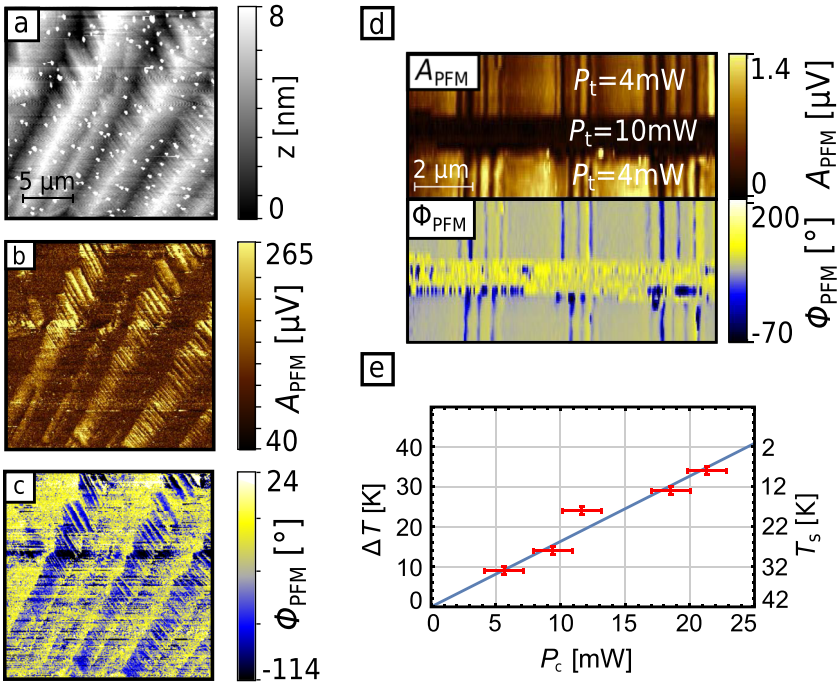

FIG. 4. Scan on the (111) surface of a GaV_4S_8 single crystal: (a) topography, (b) PFM amplitude A_{PFM}, and (c) PFM phase $_{PFM}$, displaying the lamella-shaped ferroelectric domain structure at $T_s = 20$ K. (d) An exemplarily PFM line scan at two different laser powers reveals the dis- and reappearing of ferroelectric domains at $T_s = 35$ K. (e) Linear correlation between heating T and critical laser power P_c.

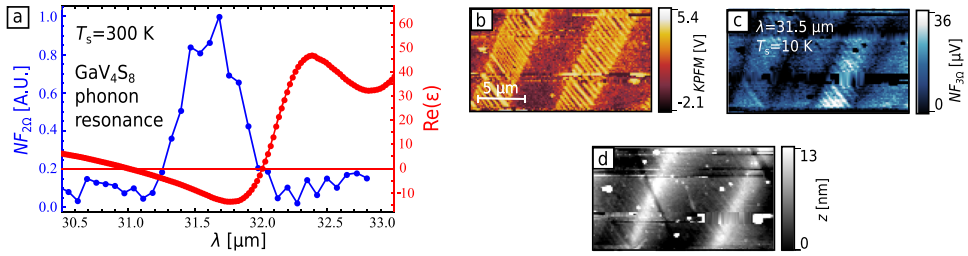

FIG. 5. Near-field study of GaV_4S_8: (a) The near-field signal NF_2 (blue) shows a distinct phonon resonance within the reststrahlen band at about 31.7 m at T_s = 300 K. The position of the resonance matches well to the permittivity " measured by Reschke *et al.*[48] with a negative Re("). In the LT-phase at T_s = 10 K, below the critical temperature, the lamella-shaped domain structure appears both in the KPFM (b) and s-SNIM (c) signals by scanning the (111) surface topography (d) of GaV_4S_8.

resulting temperature increase due to power-dependent sample heating. Figure 4(d) exemplarily displays such line scans with vanishing domains upon IR illumination. We note that the reappearing domain pattern is probably highly influenced by the ferroelectric boundaries of the heated paraelectric spot. This laser-induced local heating therefore often fully reproduces or strongly correlates with the initial domain structure, depending on the size of the spot heated above the transition temperature. The systematic analysis of controlled heating experiments will be the aim of a future publication. By setting different starting temperatures T_s, we find a linear dependence of T on P_c for the measured temperature range and extract a laser heating coefficient $\xi = T/P_c = (1.64 \quad 0.1)\ \frac{K}{mW}$ [see Fig. 4(e)]. Even though this coefficient depends on material parameters in terms of heat conductivity and absorbance, it gives a general estimation of heating effects in our specific LT s-SNIM setup for off-resonant heating far from absorption peaks.

In order to validate the heating coefficient for resonant excitation close to the reststrahlen band, we have applied the same method while operating the FEL around 31.7 μm. In this case, ξ is about 10%–15% higher as compared to the off-resonant case even though the focus diameter is about 3 times larger than with the CO_2 laser at 10.6 μm. However, no significant wavelength-dependence could be observed for the resonant case, indicating a major impact of the specific s-SNIM geometry including the metal-coated tip and cantilever on the heating, rather than absorption by the sample.

C. Near-field examination of GaV_4S_8 at T_s = 10 K

We study the local optical response of the GaV_4S_8 (111) surface in the ferroelectric phase below the Jahn-Teller transition at T_c = 42 K. Note that GaV_4S_8 is optically anisotropic where the optical axes of the different domains are parallel to the ħ111i-type directions. It has been shown earlier that such anisotropic domains may be probed in resonant s-SNIM[17,47] at specific wavelengths within the reststrahlen band of the material, making use of the strong IR-active phonon F_2 at a wavelength of about 32 μm or 310 cm ^{1}.[48,49]

For GaV_4S_8, such a resonance in the near field occurs at around λ = 31.7 μm resulting in an enhanced s-SNIM signal as shown in Fig. 5(a) for a temperature of T_s = 300 K. At the same wavelength, the permittivity Re(ε) gets negative[48] which is crucial for observing a strong resonance in the near-field signal.[47] More precisely, the strongest near-field signal is expected near the LO phonon frequency of the reststrahlen band at a wavelength of about λ = 31.3 μm. The minor deviation between the peak position of the measured s-SNIM spectrum and expected peak position referring to the macroscopic spectrum by Reschke *et al.* may be due to different samples and hence surface orientations, respectively, as well as the dependence of s-SNIM on the tapping oscillation amplitude, tip radius, and the non-interferometric detection used here. Probing the sample surface within the LT-phase, we observe the typical lamella-shaped domain structure[30] in all *in situ* accessible channels for non-contact AFM, i.e., topography, KPFM, and near-field response [Figs. 5(b)–5(d)]. Considering the laser power of P_t = 12 mW, the temperature calibration discussed above determines the local sample temperature of around 30 K within the ferroelectric phase below T_c = 42 K, which is confirmed by all measured channels, topography, s-SNIM, and KPFM.

Please note that we have deliberately chosen here a structure that is known to give the same results for all channels. However, as completely different sample properties are probed with AFM, s-SNIM, and KPFM, namely, topography, local infrared-optical response, and surface potential, these techniques are complementary and in other types of samples a full comprehensive study is enabled.

IV. CONCLUSION

We have reported here a LT s-SNIM system that, in combination with the FEL as a spectrally narrow, tunable IR laser light source, is capable of operating down to 5 K over the broad wavelength range of 5–250 μm. The LT s-SNIM allows for sub-diffraction limited infrared optical examination with a wavelength-independent lateral resolution of about 50 nm (λ/200 at 10 μm). We demonstrate LT s-SNIM operation with respect to distance decay on a Au-film, lateral resolution on Si-SiO_2, and spectral as well as structural resolution on GaV_4S_8. Furthermore, we have calibrated the temperature impact due to local laser heating using the Jahn-Teller phase transition of GaV_4S_8. Moreover, the setup supports complementary AFM techniques such as KPFM and PFM. The combination of these measurement techniques enables far-reaching opportunities for detailed investigations of phase transitions, superconducting materials, and quantum structures on the nm length scale.

ACKNOWLEDGMENTS

The authors are grateful to the ELBE team at the Helmholtz-Zentrum Dresden-Rossendorf for the operation of the free-electron laser FELBE and for dedicated support. We thank Stephan Reschke, Franz Mayr, and Vladimir Tsurkan for providing the GaV_4S_8 crystals for the calibration study and for the permittivity data of GaV_4S_8. The study of GaV_4S_8 has been conducted within the framework of the Collaborative Research Center "Correlated Magnetism: From Frustration to Topology" (SFB 1143) via TP C05. We acknowledge the funding via BMBF Grant Nos. "05K10ODB," "05K10BRA," and "05K16ODA" as well as DFG No. "KE2068/2-1." The work was supported by the Cluster of Excellence "Center for Advancing Electronics Dresden (cfaed)" as well as by the joined DAAD Project No. "TKA-DAAD 152294" and also by the Deutsche Forschungsgemeinschaft (DFG) via the Transregional Research Collaboration TRR 80: From Electronic Correlations to Functionality (Augsburg–Munich–Stuttgart).

APPENDIX: Si/SiO_2-SAMPLE

The structure was first etched into Si covered by a lithographic mask. Subsequently, the trenches were filled with amorphous SiO_2 by CVD-growth. After removing the lithography mask, the sample was polished resulting in a structure with only small topography variations between Si and SiO_2 and a thickness of the embedded SiO_2 of about 400 nm.

[1]R. Hillenbrand, T. Taubner, and F. Keilmann, Nature **418**, 159 (2002).
[2]F. Huth, A. Govyadinov, S. Amarie, W. Nuansing, F. Keilmann, and R. Hillenbrand, Nano Lett. **12**, 3973 (2012).
[3]F. Kuschewski, H.-G. von Ribbeck, J. Döring, S. Winnerl, L. M. Eng, and S. C. Kehr, Appl. Phys. Lett. **108**, 113102 (2016).
[4]M. A. Huber, F. Mooshammer, M. Plankl, L. Viti, F. Sandner, L. Z. Kastner, T. Frank, J. Fabian, M. S. Vitiello, T. L. Cocker, and R. Huber, Nat. Nanotechnol. **12**, 207 (2016).
[5]I. Amenabar, S. Poly, M. Goikoetxea, W. Nuansing, P. Lasch, and R. Hillenbrand, Nat. Commun. **8**, 14402 (2017).
[6]B. Knoll and F. Keilmann, Opt. Commun. **182**, 321 (2000).
[7]G. X. Ni, L. Wang, M. D. Goldflam, M. Wagner, Z. Fei, A. S. McLeod, M. K. Liu, F. Keilmann, B. Özyilmaz, A. H. Castro Neto, J. Hone, M. M. Fogler, and D. N. Basov, Nat. Photonics **10**, 244 (2016).
[8]L. Jiang, Z. Shi, B. Zeng, S. Wang, J.-H. Kang, T. Joshi, C. Jin, L. Ju, J. Kim, T. Lyu, Y.-R. Shen, M. Crommie, H.-J. Gao, and F. Wang, Nat. Mater. **15**, 840 (2016).
[9]P. Alonso-González, A. Y. Nikitin, Y. Gao, A. Woessner, M. B. Lundeberg, A. Principi, N. Forcellini, W. Yan, S. Vélez, A. J. Huber, K. Watanabe, T. Taniguchi, F. Casanova, L. E. Hueso, M. Polini, J. Hone, F. H. L. Koppens, and R. Hillenbrand, Nat. Nanotechnol. **12**, 31 (2016).
[10]P. Patoka, G. Ulrich, A. E. Nguyen, L. Bartels, P. A. Dowben, V. Turkowski, T. S. Rahman, P. Hermann, B. Kastner, A. Hoehl, G. Ulm, and E. Ruhl, Opt. Express **24**, 1154 (2016).
[11]T. Taubner, D. Korobkin, Y. Urzhumov, G. Shvets, and R. Hillenbrand, Science **313**, 1595 (2006).
[12]S. C. Kehr, Y. M. Liu, L. W. Martin, P. Yu, M. Gajek, S.-Y. Yang, C.-H. Yang, M. T. Wenzel, R. Jacob, H.-G. von Ribbeck, M. Helm, X. Zhang, L. M. Eng, and R. Ramesh, Nat. Commun. **2**, 249 (2011).
[13]M. Fehrenbacher, S. Winnerl, H. Schneider, J. Döring, S. C. Kehr, L. M. Eng, Y. Huo, O. G. Schmidt, K. Yao, Y. Liu, and M. Helm, Nano Lett. **15**, 1057 (2015).
[14]C. Westermeier, A. Cernescu, S. Amarie, C. Liewald, F. Keilmann, and B. Nickel, Nat. Commun. **5**, 4101 (2014).
[15]L. Ozyuzer, A. E. Koshelev, C. Kurter, N. Gopalsami, Q. Li, M. Tachiki, K. Kadowaki, T. Yamamoto, H. Minami, H. Yamaguchi, T. Tachiki, K. E. Gray, W.-K. Kwok, and U. Welp, Science **318**, 1291 (2007).
[16]D. Ahmad, B. H. Min, Y. I. Seo, W. J. Choi, S.-I. Kimura, J. Seo, and Y. S. Kwon, Supercond. Sci. Technol. **28**, 075002 (2015).
[17]J. Döring, H.-G. von Ribbeck, M. Fehrenbacher, S. C. Kehr, and L. M. Eng, Appl. Phys. Lett. **105**, 053109 (2014).
[18]A. S. McLeod, E. van Heumen, J. G. Ramirez, S. Wang, T. Saerbeck, S. Guenon, M. Goldflam, L. Anderegg, P. Kelly, A. Mueller, M. K. Liu, I. K. Schuller, and D. N. Basov, Nat. Phys. **13**, 80 (2016).
[19]B. Pajot, *Optical Absorption of Impurities and Defects in Semiconducting Crystals*, Springer Series in Solid-State Sciences (Springer Berlin Heidelberg, Berlin, Heidelberg, 2010), Vol. 158.
[20]I. C. Moldovan-Doyen, G. Xu, L. Greusard, G. Sevin, E. Strupiechonski, G. Beaudoin, I. Sagnes, S. P. Khanna, E. H. Linfield, A. G. Davies, R. Colombelli, and Y. De Wilde, Appl. Phys. Lett. **98**, 231112 (2011).
[21]H. U. Yang, E. Hebestreit, E. E. Josberger, and M. B. Raschke, Rev. Sci. Instrum. **84**, 023701 (2013).
[22]S. W. Wu, N. Ogawa, and W. Ho, Science **312**, 1362 (2006).
[23]N. Jiang, E. T. Foley, J. M. Klingsporn, M. D. Sonntag, N. A. Valley, J. A. Dieringer, T. Seideman, G. C. Schatz, M. C. Hersam, and R. P. Van Duyne, Nano Lett. **12**, 5061 (2012).
[24]R. Zhang, Y. Zhang, Z. C. Dong, S. Jiang, C. Zhang, L. G. Chen, L. Zhang, Y. Liao, J. Aizpurua, Y. Luo, J. L. Yang, and J. G. Hou, Nature **498**, 82 (2013).
[25]T. L. Cocker, D. Peller, P. Yu, J. Repp, and R. Huber, Nature **539**, 263 (2016).
[26]S. Li, S. Chen, J. Li, R. Wu, and W. Ho, Phys. Rev. Lett. **119**, 1 (2017).
[27]P. Milde, D. Köhler, J. Seidel, L. M. Eng, A. Bauer, A. Chacon, J. Kindervater, S. Mühlbauer, C. Pfleiderer, S. Buhrandt, C. Schütte, and A. Rosch, Science **340**, 1076 (2013).
[28]Z. Wang, E. Ruff, M. Schmidt, V. Tsurkan, I. Kézsmárki, P. Lunkenheimer, and A. Loidl, Phys. Rev. Lett. **115**, 1 (2015).
[29]I. Kézsmárki, S. Bordács, P. Milde, E. Neuber, L. M. Eng, J. S. White, H. M. Rønnow, C. D. Dewhurst, M. Mochizuki, K. Yanai, H. Nakamura, D. Ehlers, V. Tsurkan, and A. Loidl, Nat. Mater. **14**, 1116 (2015).
[30]Á. Butykai, S. Bordács, I. Kézsmárki, V. Tsurkan, A. Loidl, J. Döring, P. Milde, S. C. Kehr, and L. M. Eng, Sci. Rep. **7**, 44663 (2017).
[31]J. Döring, L. M. Eng, and S. C. Kehr, J. Appl. Phys. **120**, 084103 (2016).
[32]S. C. Schneider, S. Grafström, and L. M. Eng, Phys. Rev. B **71**, 115418 (2005).
[33]Q. Zhong, D. Inniss, K. Kjoller, and V. B. Elings, Surf. Sci. Lett. **290**, L688 (1993).
[34]A. D. Rakic, A. B. Djurisic, J. M. Elazar, and M. L. Majewski, Appl. Opt. **37**, 5271 (1998).
[35]P. Güthner and K. Dransfeld, Appl. Phys. Lett. **61**, 1137 (1992).
[36]L. M. Eng, H.-J. Güntherodt, G. A. Schneider, U. Köpke, and J. Muñoz Saldaña, Appl. Phys. Lett. **74**, 233 (1999).
[37]M. Nonnenmacher, M. P. O'Boyle, and H. K. Wickramasinghe, Appl. Phys. Lett. **58**, 2921 (1991).
[38]U. Zerweck, C. Loppacher, T. Otto, S. Grafström, and L. M. Eng, Phys. Rev. B **71**, 1 (2005).
[39]S. Shusterman, A. Raizman, A. Sher, Y. Parltiel, A. Schwarzman, E. Lepkifker, and Y. Rosenwaks, Nano Lett. **7**, 2089 (2007).
[40]Z. Schumacher, Y. Miyahara, A. Spielhofer, and P. Grutter, Phys. Rev. Appl. **5**, 1 (2016).
[41]G. Wurtz, R. Bachelot, and P. Royer, Rev. Sci. Instrum. **69**, 1735 (1998).
[42]R. Hillenbrand, M. Stark, and R. Guckenberger, Appl. Phys. Lett. **76**, 3478 (2000).
[43]S. C. Kehr, J. Döring, M. Gensch, M. Helm, and L. M. Eng, Synchrotron Radiat. News **30**, 31 (2017).
[44]D. Chandler-Horowitz and P. M. Amirtharaj, J. Appl. Phys. **97**, 123526 (2005).
[45]J. Kischkat, S. Peters, B. Gruska, M. Semtsiv, M. Chashnikova, M. Klinkmüller, O. Fedosenko, S. Machulik, A. Aleksandrova, G. Monastyrskyi, Y. Flores, and W. T. Masselink, Appl. Opt. **51**, 6789 (2012).
[46]S. Babar and J. H. Weaver, Appl. Opt. **54**, 477 (2015).
[47]S. C. Kehr, M. Cebula, O. Mieth, T. Härtling, J. Seidel, S. Grafström, L. M. Eng, S. Winnerl, D. Stehr, and M. Helm, Phys. Rev. Lett. **100**, 1 (2008).
[48]S. Reschke, F. Mayr, Z. Wang, P. Lunkenheimer, W. Li, D. Szaller, S. Bordács, I. Kézsmárki, V. Tsurkan, and A. Loidl, Phys. Rev. B **96**, 144302 (2017).
[49]J. Hlinka, F. Borodavka, I. Rafalovskyi, Z. Docekalova, J. Pokorny, I. Gregora, V. Tsurkan, H. Nakamura, F. Mayr, C. A. Kuntscher, A. Loidl, S. Bordács, D. Szaller, H. J. Lee, J. H. Lee, and I. Kézsmárki, Phys. Rev. B **94**, 1 (2016).